Addressing Grating Lobes in Linear Scanning Phased Arrays with Self-Nulling Elements and Optimized Amplitude Distributions

Zabed Iqbal and Maria Pour[*]

Abstract—An effective method to reduce grating lobes in linear scanning phased array antennas with large element spacing of one wavelength is presented. The proposed technique is based on employing self-nulling antenna elements by simultaneously exciting the first two modes in a circular microstrip patch antenna to partially nullify the grating lobes. More importantly, a modified amplitude tapering is optimized in the array level to facilitate the grating lobe reduction for relatively wide scan angles up to $\pm 60°$. Analytical results of a 21-element linear array are fully presented, and a $-22.5\,\text{dB}$ grating lobe reduction for up to $\pm 60°$ scan angles is reported using the proposed method, followed by the results of a smaller array for validation purposes.

1. INTRODUCTION

Scanning phased array antennas are much sought after in modern wireless communication systems because they can provide high directivity, reconfigurable radiation patterns, moderate aperture efficiency, and electronic beam scanning [1]. Microstrip patch antennas have extensively been used as an element in phased arrays due to their easy fabrication and accessible integration with the feeding network and other microwave circuits. The main drawback of conventional patch antennas is their low efficiency, which results in limited gain in the order of 5–6 dBi for a single element [2]. To simultaneously reduce the cost of phased array antennas and increase gain, a substantially large aperture area with a reduced number of elements is required, which inherently necessitates the use of large inter-element spacing. However, grating lobes appear in the visible region for element spacing greater than half a wavelength, which worsens for medium- and wide-scanned beams [3].

Various grating lobe reduction techniques have been reported to improve the phased array performance. The sparse or thinned array [4, 5] is one of the most common approaches to reduce grating lobes. However, building a large thinned array is challenging and cumbersome as it often needs complicated optimization techniques [6–8] and feeding networks to achieve desired radiation characteristics. Another classical approach to suppress grating lobes is the aperiodic distribution of the elements [9] or subarrays [10, 11] with a tapered amplitude excitation. To this end, non-uniform element separation [12] along with an amplitude tapering was used to reduce grating lobes [13] as well as minor lobes [14]. In addition, the desired minor lobes can be obtained by using different array synthesis methods, e.g., orthogonal [15], Tschebyscheff [16–18], and binomial arrays [19, 20]. However, all of the aforementioned grating lobe reduction methods and array syntheses use conventional single-mode antennas as an element. In contrast, adaptive multi-mode antenna elements exhibit unique self-scanning and nulling characteristics, which have been utilized by the authors in hexagonal planar phased arrays [21, 22] to reduce grating lobes for small-, medium-, and wide-scan angles by uniformly tapering the amplitude coefficients of the peripheral elements. Recently, preliminary results of grating

The authors are with the Department of Electrical and Computer Engineering, The University of Alabama in Huntsville, Huntsville, AL 35899, USA.

lobe reductions in a planar array using the dual-mode elements for scan angles up to $45°$ were presented by the authors in [23], wherein the standard $-30\,\text{dB}$ Tschebyscheff distribution was applied to the array without any further optimization.

In this paper, the grating lobe issue is further addressed in linear scanning phased array antennas, consisting of dual-mode microstrip patch elements, spaced one-wavelength apart, for scanned angles up to $\pm 60°$. The dual-mode circular microstrip patch antenna operates at the TM_{11} and TM_{21} modes. It will be shown that in addition to using the adaptive dual-mode elements, the amplitude distribution of the array is no longer a simple step function as reported in [21] in hexagonal planar arrays; instead it needs to be properly optimized to mitigate the grating lobe issues. To this end, a 21-element linear phased array is investigated. It will be shown that the grating lobes reduce to well below $-22.5\,\text{dB}$ for the scan angles up to $\pm 60°$. The array performance in terms of grating lobes is compared with conventional amplitude tapering distributions such as the Binomial and Tschebyscheff ones in counterpart arrays consisting of single-mode antenna elements. For the proof of concept, the simulated and synthesized measured patterns are provided for an 11-element linear array with the $30°$ scan angle and an element spacing of one wavelength.

2. ANALYTICAL MODEL OF THE ELEMENT AND ARRAY

Based on the cavity model, a dual-mode circular microstrip patch antenna, which is the constitutive element of the proposed phased array antenna, is analyzed at the frequency of $10\,\text{GHz}$. A two-layer stacked configuration supported by an infinite ground plane was adopted to construct such a dual-mode antenna element as depicted in Fig. 1. For simplicity, air ($\varepsilon_r = 1$) is considered as the dielectric substrate with a thickness of $0.053\lambda_o$ between the layers. The TM_{11} mode was exited in the top patch with radius $a_1 = 0.293\lambda_o$ and the TM_{21} mode was excited in the middle patch with radius $a_2 = 0.486\lambda_o$, where λ_o is the free-space wavelength at $10\,\text{GHz}$.
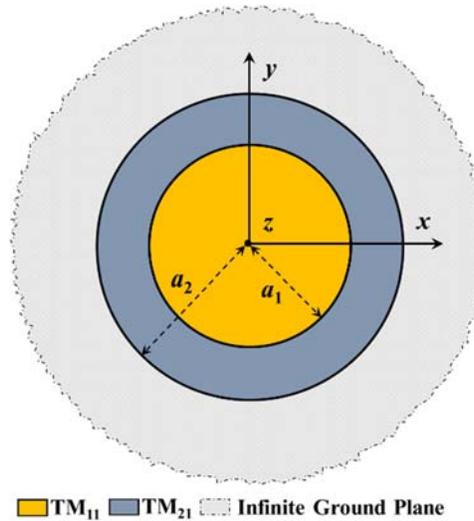

Figure 1. Top-view of the dual-mode circular microstrip patch antenna element operating at the TM_{11} and TM_{21} modes with $a_1 = 0.293\lambda_o$ and $a_2 = 0.486\lambda_o$, where λ_o is the free-space wavelength at $10\,\text{GHz}$.

As expected, the microstrip patch antenna generates broadside and conical radiation patterns at the individual TM_{11} and TM_{21} modes [24], respectively. To demonstrate the self-scanning and adaptive nulling [25] properties of the dual-mode circular patch antenna, some representative element patterns of the combined modes with a $+90°$ phase shift are plotted in Fig. 2(a) for different magnitudes of the mode excitation ratio, denoted by $|A_{21}|$, which represents the relative strength of the TM_{21} mode to that of the dominant TM_{11} mode. The phase shift between the two modes is denoted by α_{21}. That is, $A_{21} = |A_{21}|\angle\alpha_{21}$. As observed in Fig. 2(a), the main beam direction and the location of nulls of
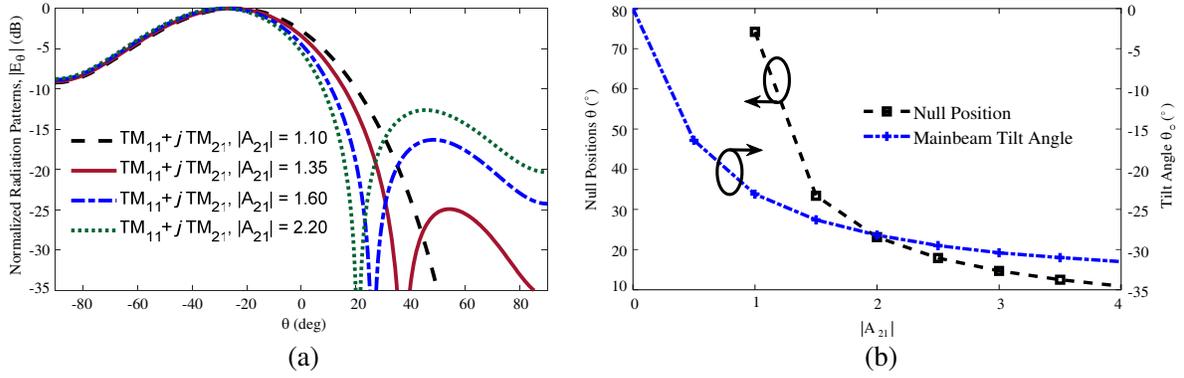
Figure 2. (a) Normalized radiation patterns, (b) null positions and tilt angle of a circular microstrip patch antenna operating at the combined TM_{11} and TM_{21} modes with a $90°$ phase shift for different $|A_{21}|$.

the element patterns are controlled by the magnitude excitation ratio $|A_{21}|$, while a $+90°$ phase shift between the two modes is required to form a full null in the element pattern. More specifically, the main beam of the element pattern is scanned towards positive and negative elevation angles, for phase shifts of $-90°$ and $+90°$, respectively. For brevity, only the results for the latter phase shift are plotted in Fig. 2(a). Thus, by simultaneously exciting the two modes, a null is formed in the element pattern, which can be steered by the magnitude excitation ratio $|A_{21}|$ to partially nullify the grating lobe in the array pattern. In the element level, a continuous null steering from $10°$ to $74°$ is realized by changing $|A_{21}|$ from 4.0 to 1.0, resulting in a $64°$ dynamic null range. Also, the main beam scans from broadside to $-32°$ for $|A_{21}|$ from 0 to 4.0, as per Fig. 2(b).

As an example, a 21-element linear array is investigated, which is composed of identical dual-mode circular microstrip patch antenna elements placed symmetrically along the x-axis with an element spacing of $d = \lambda_o$, as illustrated in Fig. 3. The total radiation pattern of the linear array is expressed by [3],

$$\mathbf{E}_t(\theta, \phi) = \mathbf{E}_{element}(\theta, \phi) \times AF(\theta, \phi) \tag{1}$$

where $\mathbf{E}_t(\theta, \phi)$ is the total array radiation pattern, $\mathbf{E}_{element}(\theta, \phi)$ the element pattern, and $AF(\theta, \phi)$ the array factor of the 21-element linear array, which can be written as,

$$AF(\theta, \phi) = \sum_{r=1}^{M+1} w_r \cos\left[\frac{2\pi d(r-1)}{\lambda}(\sin\theta\cos\phi - \sin\theta_o\cos\phi_o)\right] \tag{2}$$

and,

$$\mathbf{E}_{element}(\theta, \phi) = \hat{\mathbf{a}}_{\boldsymbol{\theta}} E_\theta(\theta, \phi) + \hat{\mathbf{a}}_{\boldsymbol{\phi}} E_\phi(\theta, \phi) \tag{3}$$

$$\begin{aligned} E_\theta(\theta, \phi) = & -j\left([J_0(k_o a_1 \sin\theta) - J_2(k_o a_1 \sin\theta)]\cos\phi \right. \\ & \left. +jA_{21}[J_1(k_o a_2 \sin\theta) - J_3(k_o a_2 \sin\theta)]\cos 2\phi\right) \end{aligned} \tag{4}$$

$$\begin{aligned} E_\phi(\theta, \phi) = & +j\left([J_0(k_o a_1 \sin\theta) + J_2(k_o a_1 \sin\theta)]\sin\phi \right. \\ & \left. +jA_{21}[J_1(k_o a_2 \sin\theta) + J_3(k_o a_2 \sin\theta)]\sin 2\phi\right)\cos\theta \end{aligned} \tag{5}$$
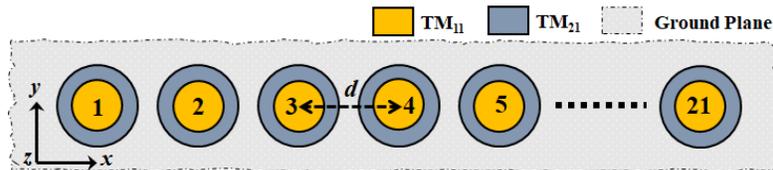

Figure 3. Geometry of a 21-element linear phased array consisting of the proposed dual-mode circular patch antennas with element spacing of $d = \lambda_o$.

In Eq. (2), w_r is the amplitude coefficient of the array elements, and (θ_o, ϕ_o) are the angular location of the scanned beam, and $M = 10$ for the 21-element linear array. In Eqs. (4)–(5), k_o is the wave number, and a_1 and a_2 are the radii of the TM$_{11}$ and TM$_{21}$ patches, respectively. $J_m(u)$ is the Bessel function of the first kind of order mth, where m changes from 0 to 3. The zeros of the derivatives of the Bessel function determine the order of the resonant frequencies and the effective radii of the patches.

3. OPTIMIZED AMPLITUDE DISTRIBUTION

Radiation patterns with low grating lobes (GL) and sidelobe levels (SLL) are highly sought after in many applications, e.g., wide-angle scanning radars, passive multifunctional imaging radars, automotive radars such as collision avoidance, autonomous cruise control radars and many more. While low SLL arrays can be synthesized by properly tapering the amplitude distributions of the elements, grating lobes cannot necessarily be reduced by only empowering tapered amplitude distributions. Thus, to reduce grating lobes effectively, an element pattern with self-nulling characteristics is required, which can be realized by simultaneously exciting the TM$_{11}$ and TM$_{21}$ modes in circular patch elements. In particular, a proper mode excitation ratio of A_{21} needs to be utilized for a given scan angle, as it controls the main beam tilt angles and element pattern nulls. The direction of the scanning beam in the element level is controlled by the polarity of the $\pm 90°$ phase shift between the modes. Thus, the main parameters to reduce the grating lobes are the magnitude excitation ratio of $|A_{21}|$ and array coefficients w_r. In this study, the Genetic Algorithm (GA) optimization tool [26] in MATLAB is used to find the optimal values of $|A_{21}|$ and w_r for a given scan angle for the realization of maximum grating lobe reduction and low SLLs in linear arrays with one-wavelength element spacing.

In the GA, the initial population was chosen as 200 chromosomes, and each chromosome consists of $(N+1)/2$ genes. Of these $(N+1)/2$ genes, $(N-1)/2$ genes contain the information of the amplitude distribution of the N elements, and one gene represents $|A_{21}|$. In this study, without the loss of generality, an odd number of elements, e.g., $N = 11$, 15, or 21, are considered, in which the amplitude coefficient of the elements is normalized to that of the centre element. Now, to evolve toward the optimal values of the $|A_{21}|$ and w_r, a fitness function (FF) is defined as,

$$FF = q_1 \cdot |GL_t(\theta_o) - GL(\theta_o)| + q_2 \cdot |SLL_t - SLL| \tag{6}$$

where GL_t and SLL_t are the target grating lobe and target SLL, respectively, while q_1 and q_2 are the respective weights. The target SLL was set to $-40\,$dB. The expected grating lobe is a function of scan angle θ_o, and thus the minimum grating lobe was set to $-30\,$dB for $\theta_o = -60°$. Adaptive feasible mutation and a crossover fraction of 0.8 were used as reproduction criteria. The maximum generation is $25 \times (N+1)$, which was set as the stopping criterion. The constrains on the amplitude tapering were bounded such that its upper and lower limits were set to the $-30\,$dB Tschebyscheff and the standard Binomial distributions, respectively. The normalized Binomial coefficients for an N (odd) element linear array can be calculated by,

$$w_r^B = \frac{\left(\frac{n}{2}!\right)^2}{(r-1)!\,(n-r+1)!} \tag{7}$$

where $r = 1, 2, \ldots, n+1$, and $n = N - 1$. The optimized amplitude coefficients (w_r) and $|A_{21}|$ for different scan angles in the 21-element linear phased array with one-wavelength element spacing are provided in Fig. 4.

4. RESULTS: RADIATION PATTERNS, ARRAY DISTRIBUTIONS, AND DIRECTIVITY

To verify the proposed grating lobe reduction method using the dual-mode antenna element with the optimized amplitude tapering of the array, results for different scan angles are presented and discussed for the 21-element linear array shown in Fig. 3. To further demonstrate the capability of the proposed technique, the dual-mode array with the optimized amplitude tapering is compared with the conventional arrays of single-mode elements with standard Binomial and $-40\,$dB Tschebyscheff
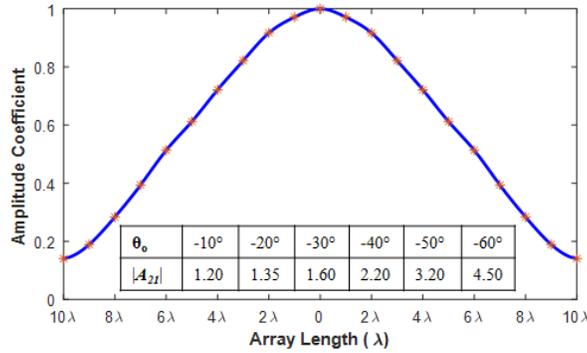
Figure 4. GA optimized values of the amplitude coefficients (w_r) of the 21-element array when $d = \lambda_o$. (Inset — GA optimized values of the mode excitation ratios for a given scan angle).

distributions for the respective scan angle, maintaining a one-wavelength element spacing for all cases. The corresponding results for the scan angles of $-20°$, $-40°$ and $-60°$ are shown in Figs. 5(a)–(c), respectively. As can be seen, for the $-20°$ scan angle, the grating lobe for the dual-mode ($A_{21} = 1.35/90°$) case is reduced to well below -30 dB with the optimized amplitude distribution. The reduction is in order of -31 dB when the main beam is scanned to $-40°$ with the same set of amplitude tapering coefficients and $|A_{21}| = 2.2$, as depicted in Fig. 5(b). Interestingly enough, even for the wide scan angle of $-60°$, a 22.5 dB grating lobe reduction is realized with the proposed method,
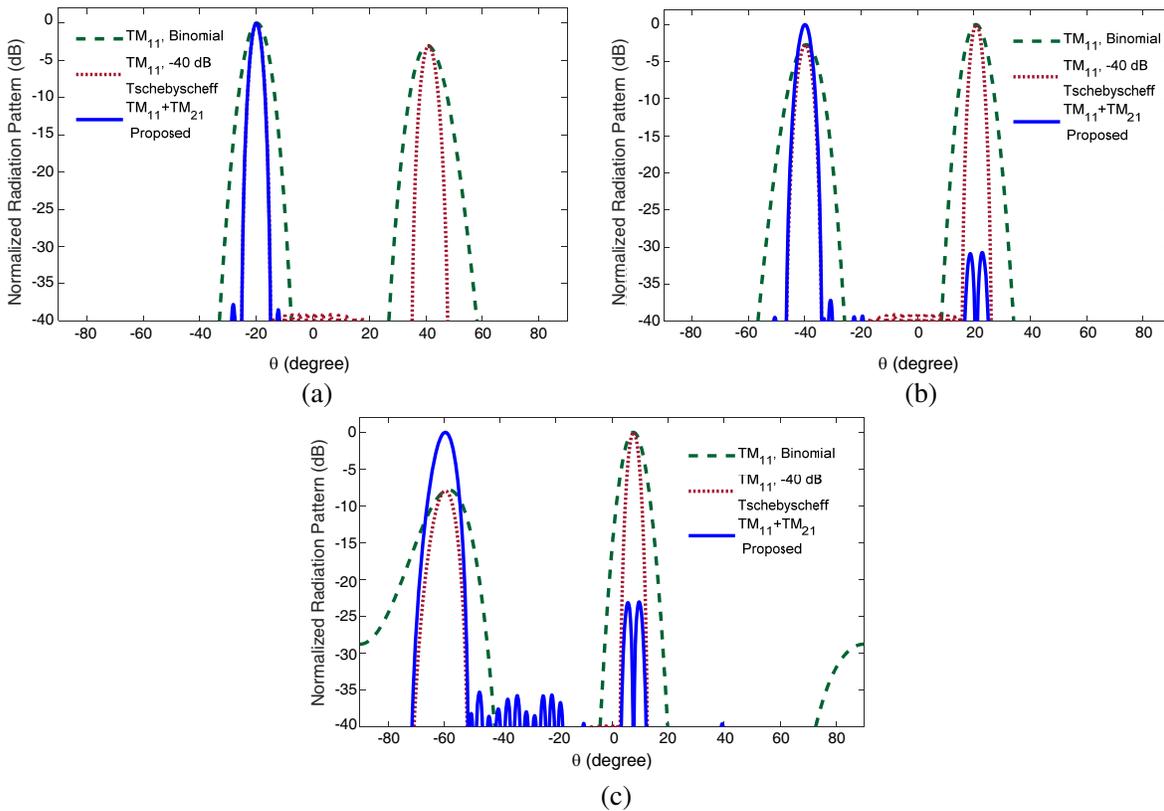

Figure 5. Normalized radiation patterns of the 21-element linear phased array with $d = \lambda_o$, for the scan angle of (a) $\theta_o = -20°$, (b) $\theta_o = -40°$ and (c) $\theta_o = -60°$, with both single-mode antenna elements with Binomial and -40 dB Tschebyscheff excitations, and the dual-mode antenna elements with optimized amplitude distribution; for dual-mode cases: (a) $|A_{21}| = 1.35$, (b) $|A_{21}| = 2.2$, and (c) $|A_{21}| = 4.5$.

when $|A_{21}| = 4.5$. Several minor lobes appear in the radiation patterns as per Fig. 5(c), though all of which are well below -35 dB. These minor lobes can be further suppressed by choosing another set of tapering coefficients, which are close to the regular Binomial expansion, but with the penalty of larger far-out lobes. The corresponding results are omitted here for brevity. It is worth noting that the grating lobes are almost as high as the main beam for the conventional single-mode arrays with standard Binomial and -40 dB SLL Tschebyscheff amplitude distributions for the aforementioned scan angles, as shown in Fig. 5. This implies that tapering off the amplitude distribution in conventional, single-mode, scanning linear arrays to reduce grating lobes simply becomes ineffective. Instead, adaptive antenna elements with null-steering capabilities, such as the proposed dual-mode elements, are required.

A sequence of normalized radiation patterns of the optimized 21-element linear phased array antenna is plotted in Fig. 6, starting from $\theta_o = -10°$ to $\theta_o = -60°$, when $d = \lambda_o$. All the grating lobes of the total radiation patterns, i.e., the product of the antenna element and the array factor, have been reduced to well below -22.5 dB.
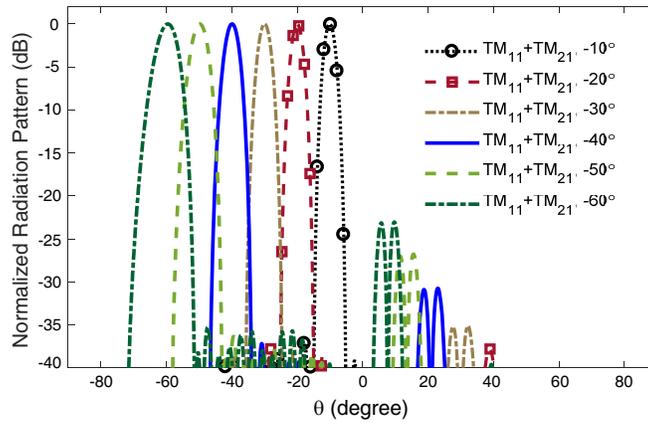

Figure 6. Normalized radiation patterns of the optimized 21-element linear phased array with $d = \lambda_o$, and a scan angle from $\theta_o = -10°$ to $\theta_o = -60°$, with the dual-mode antenna elements and modified array amplitude coefficients.

The proposed modified amplitude coefficients are compared with the conventional amplitude functions, i.e., uniform, Binomial, and -30 dB and -40 dB Tschebyscheff in Figs. 7(a)–(c) for 11-, 15-, and 21-element linear arrays, respectively. The optimized coefficients for the scan angle up to $-60°$ with one-wavelength element spacing are quite close to those of the classical -39.2 dB Tschebyscheff synthesis, as illustrated in Fig. 7.

Figure 8 summarizes the resultant grating lobe reduction and the required $|A_{21}|$ of the proposed method for the scan angles of $-10°$ to $-60°$, with one-wavelength element spacing. It is seen that the grating lobes are reduced to well below -22.5 dB by using the dual-mode self-nulling elements and optimizing their amplitude coefficients in the array level. The selection of null positions, along with the scanned main beam angle, is crucial to effectively reduce the grating lobes. More specifically, the mode excitation ratio controls the element pattern shapes and the positions of the nulls in order to partially nullify the grating lobes for a given scan angle.

It is also interesting to note in Fig. 5 that the beamwidth of the optimized dual-mode array now slightly decreases compared to that of conventional single-mode arrays. This will in turn result in lesser gain drop as the main beam scans away from the boresight angle in the proposed dual-mode antenna array. For further clarification, the directivity versus scan angles for the 21-element linear array is plotted in Fig. 9. As observed, the directivity of the dual-mode array is greater than that of the conventional single-mode arrays with the -40 dB Tschebyscheff and Binomial amplitude distributions. Moreover, as the beam scans from $\theta_o = 10°$ to $\theta_o = 60°$, the relative gain drop is only 2.5 dB in the proposed dual-mode array, which is impressively less than the ~ 6 dB gain drop in the conventional Binomial and -40 dB Tschebyscheff arrays, as shown in Fig. 9.
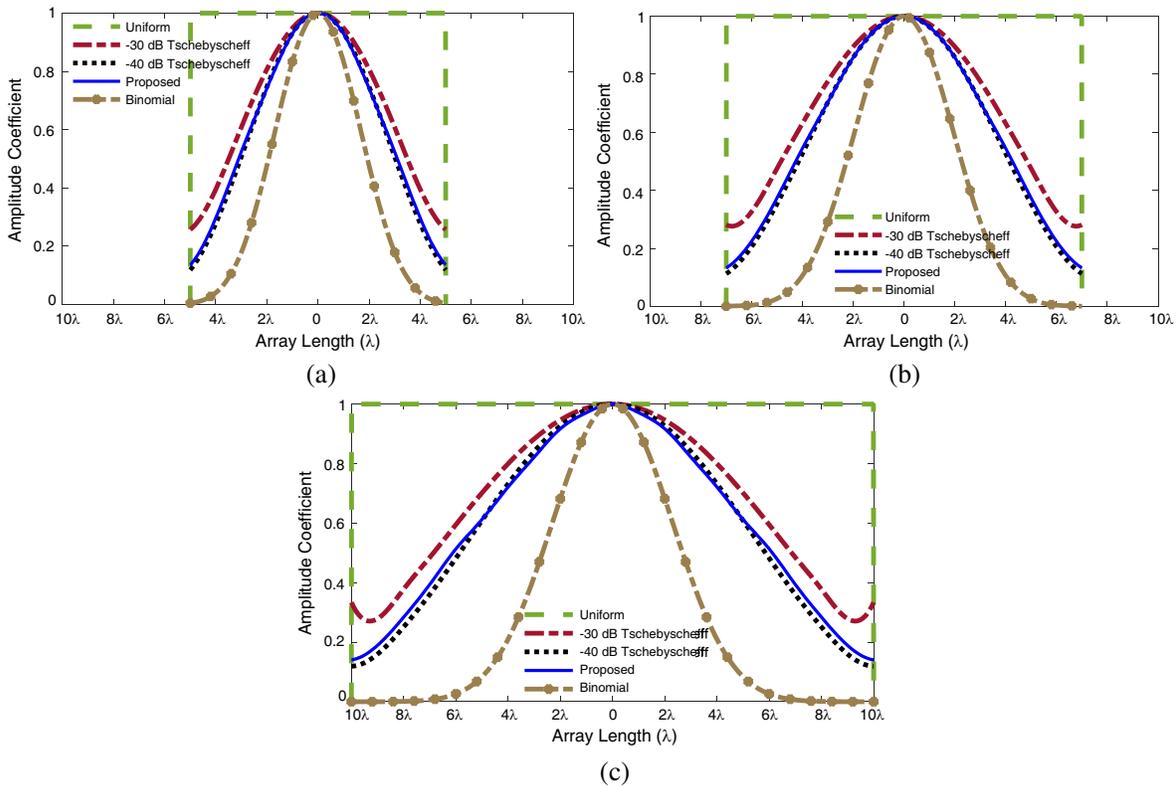
Figure 7. Comparison of proposed amplitude distribution with other standard amplitude distributions versus array length for (a) 11-element, (b) 15-element and (c) 21-element linear phased arrays with $d = \lambda_o$.
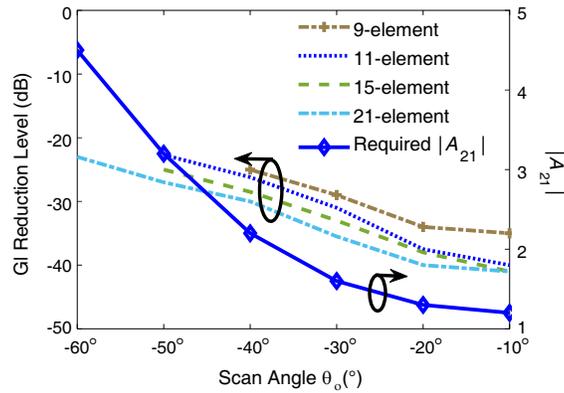

Figure 8. Grating lobe reduction level versus scan angles of the 9-, 11-, 15-, and 21-element linear phased arrays with $d = \lambda_o$. (Right Axis: mode excitation ratio versus scan angles).

5. FULL-WAVE AND MEASURED RESULTS

To include the edge effect and the mutual coupling between the elements and the modes, which were ignored in the analytical results in Section 4, a full-wave simulation was carried out in the array level. To validate the proposed grating lobe reduction method and in the interest of computational time and without the loss of generality, a smaller 11-element linear phased array consisting of the dual-mode antenna elements with one-wavelength element spacing is simulated using finite-element method based
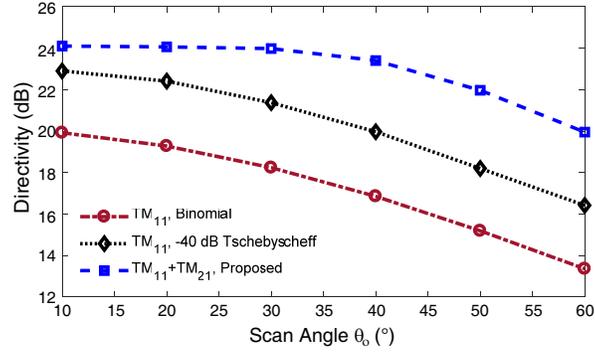
Figure 9. Directivity versus scan angles of the proposed 21-element dual-mode linear array with $d = \lambda_o$, compared with its counterpart single-mode arrays with Binomial and -40 dB Tschebyscheff distributions.
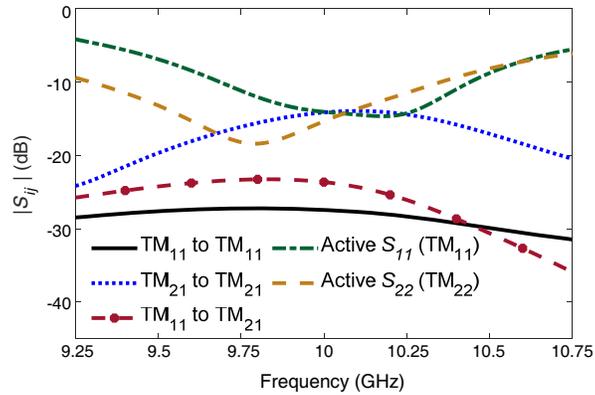

Figure 10. Active S-parameters and mutual coupling between the adjacent elements of the 11 element linear phased array antenna with $d = \lambda_o$.

full-wave EM solver ANSYS HFSS [27]. The arrangement of the dual-mode antenna element is similar to that of the dual-mode microstrip patch antenna reported by the authors in [28]. Representative results of simulated active scattering parameters of the dual-mode 11-element linear array are shown in Fig. 10, where the active S_{11} and S_{22} are the active reflection coefficients of the ports exciting the TM_{11} and TM_{21} modes, respectively. Good impedance matching is observed for the both TM_{11} and TM_{21} modes as active $|S_{11}|$ and $|S_{22}|$ are below -15 dB at the design frequency of 10 GHz. In the array level, the associated mutual couplings are categorized into two major groups: (a) mutual coupling between two adjacent elements and (b) mutual coupling among non-adjacent elements. More specifically, each group represents mutual coupling between (i) TM_{11} to TM_{11} modes (ii) TM_{21} to TM_{21} modes, and (iii) TM_{11} to TM_{21} modes and vice versa. As shown in Fig. 10, the highest mutual coupling occurs between the TM_{21} modes amongst the adjacent elements, which is below -15 dB at 10 GHz.

To show the grating lobe reduction capability of the proposed dual-mode method in the 11-element linear phased array with one-wavelength element spacing, proper mode excitation ratios and optimized amplitude distributions were applied to each element. The results are depicted in Fig. 11 for the scan angle of $30°$. As can be seen, a grating lobe as high as the main lobe is emerged in the $-30°$ scan angle in the uniformly-excited, single-mode array. In contrast, by employing the optimized dual-mode antenna elements, the grating lobe reduces to -20 dB with this large element spacing of one wavelength both in full-wave simulation and synthesized measured patterns. For the $30°$ scan angle, the simulated peak gain and realized gain of the proposed dual-mode, 11-element phased array are 19.7 dBi and 17.3 dBi, respectively, whereas the conventional single-mode, 11-element phased array counterpart exhibits the peak gain of 17.5 dBi and the peak realized gain of 16.2 dBi. The measured pattern for the 11-element array is obtained by directly multiplying the measured radiation pattern of the fabricated dual-mode
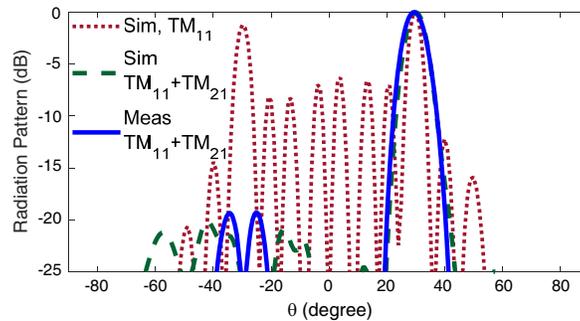
Figure 11. Normalized radiation patterns of the 11-element linear phased arrays with conventional single TM_{11} mode excitation with uniform amplitude distribution, and simulated and synthesized measured patterns of the dual-mode $TM_{11} + TM_{21}$ excitation with modified amplitude tapering for a scan angle of $30°$, when $d = \lambda_o$.

circular microstrip patch antenna in [28] with the array factor. As per the analytical results in Fig. 8, the grating lobe reduction for the 11-element linear array using the proposed method was around -28 dB. The discrepancy between the analytical and full-wave or measured results is mainly due to probes and mutual coupling, which were ignored in the analytical investigation. Nonetheless, such a grating lobe reduction is quite significant in phased array antennas with one-wavelength element spacing.

6. CONCLUSION

The grating lobe reduction in linear scanning arrays with one-wavelength element spacing was addressed. The arrays comprising conventional single-mode elements suffer from large grating lobes. It was shown that by optimizing the array excitation coefficients and utilizing dual-mode elements with self-scanning and adaptive nulling properties, the grating lobe could be reduced significantly. The main idea is to judiciously choose the mode excitation ratio in the antenna element, which facilitates steering the position of the element pattern null close to that of the grating lobe, as well as properly optimize the amplitude tapering coefficients in the array level to effectively reduce the grating lobes and SLLs. A -22.5 dB grating lobe reduction was achieved for a $-60°$ scan angle with one-wavelength element spacing. This novel technique exhibited promising results on grating lobe reductions and gain enhancement over the conventional single-mode antenna arrays excited by standard Binomial and Tschebyscheff amplitude distributions.

ACKNOWLEDGMENT

REFERENCES

1. Fourikis, N., *Phased Array-based Systems and Applications*, John Wiley & Sons, New York, 1997.
2. Garg, R., P. Bhartia, I. J. Bahl, and A. Ittipiboon, *Microstrip Antenna Design Handbook*, Artech House, 2001.
3. Balanis, C. A., *Antenna Theory: Analysis and Design*, 4th edition, Wiley, Hoboken, 620 NJ, USA, 2016.
4. Yu, J., V. A. Khlebnikov, and M.-H. Ka, "Wideband grating-lobe suppression by rotation of the phased array stations in the SKA low-frequency sparse aperture array," *IEEE Trans. Antennas Propag.*, Vol. 63, No. 9, 393–3946, Sept. 2015.

5. Tu, X., G. Zhu, X. Hu, and X. Huang, "Grating lobe suppression in sparse array-based ultrawideband through-wall imaging radar," *IEEE Antennas Wireless Propag. Lett.*, Vol. 15, 1020–1023, Oct. 2016.

6. Zhao, X., Q. Yang, and Y. Zhang, "A hybrid method for the optimal synthesis of 3-D patterns of sparse concentric ring arrays," *IEEE Trans. Antennas Propag.*, Vol. 64, No. 2, 515–524, Feb. 2016.

7. Goudos, S. K., K. Siakavara, T. Samaras, E. E. Vafiadis, and J. N. Sahalos, "Sparse linear array synthesis with multiple constraints using differential evolution with strategy adaptation," *IEEE Antennas Wireless Propag. Lett.*, Vol. 10, 670–673, Jul. 2011.

8. Chen, K., H. Chen, L. Wang, and H. Wu, "Modified real GA for the synthesis of sparse planar circular arrays," *IEEE Antennas Wireless Propag. Lett.*, Vol. 15, 274–277, Jun. 2015.

9. Lu, B., S. X. Gong, S. Zhang, Y. Guan, and J. Ling, "Optimum spatial arrangement of array elements for suppression of grating-lobes of radar cross section," *IEEE Antennas Wireless Propag. Lett.*, Vol. 9, 114–117, Feb. 2010.

10. Bianchi, D., S. Genovesi, and A. Monorchio, "Randomly overlapped subarrays for reduced sidelobes in angle-limited scan arrays," *IEEE Antennas Wireless Propag. Lett.*, Vol. 16, 1969–1972, Apr. 2017.

11. Krivosheev, Y. V., A. V. Shishlov, and V. V. Denisenko, "Grating lobe suppression in aperiodic phased array antennas composed of periodic subarrays with large element spacing," *IEEE Antennas Propag. Magazine*, Vol. 57, No. 1, 76–85, Feb. 2015.

12. Harrington, R. F., "Sidelobe reduction by nonuniform element spacing," *IRE Trans. Antennas Propag.*, Vol. 9, No. 2, 187–192, Mar. 1961.

13. Haupt, R. L., "Reducing grating lobes due to subarray amplitude tapering," *IEEE Trans. Antennas Propag.*, Vol. 9, No. 8, 846–850, Aug. 1985.

14. Diawuo, H. A., S. J. Lee, and Y.-B. Jung, "Sidelobe-level reduction of a linear array using two amplitude tapering techniques," *IET Microwave Antennas Propag.*, Vol. 11, No. 10, 1432–1437, Jul. 2017.

15. Goudos, S. K., G. S. Miaris, K. Siakavara, and J. N. Sahalos, "On the orthogonal nonuniform synthesis from a set of uniform linear arrays," *IEEE Antennas Wireless Propag. Lett.*, Vol. 6, 313–316, Jul. 2007.

16. Koretz, A. and B. Rafaely, "Dolph-Chebyshev beampattern design for spherical arrays," *IEEE Trans. Antennas Propag.*, Vol. 57, No. 6, 2417–2420, Jun. 2009.

17. Buttazzoni, G. and R. Vescovo, "Gaussian approach versus Dolph-Chebyshev synthesis of pencil beams for linear antenna arrays," *Electronic Lett.*, Vol. 54, No. 1, 8–10, Jan. 2018.

18. Abreu, G. T. F. and R. Kohno, "A Modified Dolph-Chebyshev approach for the synthesis of low sidelobe beampatterns with adjustable beamwidth," *IEEE Trans. Antennas Propag.*, Vol. 51, No. 10, 3014–3017, Oct. 2003.

19. Juntunen, J. O., K. I. Nikoskinen, and K. J. M. Heiska, "Binomial array as a multistate phase diversity antenna," *IEEE Trans. Vehicular Tech.*, Vol. 49, No. 3, 698–705, May 2000.

20. Ling, C.-W., W.-H. Lo, R.-H. Yan, and S.-J. Chung, "Planar binomial curved monopole antennas for ultrawideband communication," *IEEE Trans. Antennas Propag.*, Vol. 55, No. 9, 2622–2624, Sept. 2007.

21. Iqbal, Z. and M. Pour, "Grating lobe reduction in scanning phased array antennas with large element spacing," *IEEE Trans. Antennas Propag.*, Vol. 66, No. 12, 6965–6974, Dec. 2018.

22. Iqbal, Z. and M. Pour, "Exploiting higher order modes for grating lobe reductions in scanning phased array antennas," *IEEE Trans. Antennas Propag.*, Vol. 67, No. 11, 7144–7149, Aug. 2019.

23. Iqbal, Z. and M. Pour, "Grating lobe mitigation in scanning planar phased array antennas," *IEEE Int. Symp. Phased Array Systems and Tech.*, 1–3, Waltham, MA, USA, Oct. 15–18, 2019.

24. Haung, J., "Circularly polarized conical patterns from circular microstrip antennas," *IEEE Trans. Antennas Propag.*, Vol. 32, No. 9, 991–994, Sept. 1984.

25. Iqbal, Z. and M. Pour, "Amplitude control null steering in a multi-mode patch antenna," *Progress In Electromagnetics Research Letters*, Vol. 82, 107–112, 2019.

26. GA Toolbox, MATLAB 2017, The MathWorks, Inc., Natick, Massachusetts, United States, [online] Available: https://www.mathworks.com/products/global-optimization.html.

27. "High frequency structure simulator (HFSS 18.0)," Canonsburg, PA, USA, ANSYS, 2018.

28. Pour, M., M. Henley, A. Young, and Z. Iqbal, "Cross-polarization reduction in offset reflector antennas with dual-mode microstrip primary feeds," *IEEE Antennas and Wireless Propag. Lett.*, Vol. 18, No. 5, 926–930, Mar. 2019.